INTERMEDIATE TRANSPORT IN NANOSCALE SCAFFOLDS FOR MULTISTEP CATALYTIC REACTIONS

By

Erica Earl

A THESIS

Submitted to
Michigan State University
in partial fulfillment of the requirements
for the degree of

Chemical Engineering- Master of Science

2016

ABSTRACT

INTERMEDIATE TRANSPORT IN NANOSCALE SCAFFOLDS FOR MULTISTEP CATALYTIC REACTIONS

By

Erica Earl

Efficient catalytic cascades that involve several sequential reactions are found frequently in nature. The efficiency of multi-step biochemical pathways is enhanced by substrate channeling, wherein the product of one reaction is directed toward and acts a substrate to the next sequential reaction. This mechanism can partially overcome diffusion, which is often fast compared to reaction rates, and promotes loss of intermediates. Substrate channeling is achieved by the architecture and scaffolding of biological molecules, and mimicking these natural structures could lead to innovative catalyst designs. We investigate the efficiency of two channeling approaches – electrostatic interactions and surface adsorption – through continuum modeling, to identify the limits of these modes and the extent to which they can interact. The model considers transport between two active sites where an intermediate is produced at the first active site and consumed at the second. The system includes mass transport through diffusion and migration, and reaction kinetics at the active sites. The effectiveness of this model is quantified by yield of the second reaction and by flux control coefficients (FCCs). Controlling the proximity between active sites, and surface adsorption are found to be inefficient as high rate constants are required to obtain significant yields. The introduction of electrostatic interactions, however, leads to yields of over 90% at low rate constants.

ACKNOWLEDGEMENTS

I would like to acknowledge my advisor and colleagues for their mentorship and support. I would also like to acknowledge my funding sources which have included The Army Research Office, The Sloan Engineering Program, and the State of Michigan through the Department of Chemical Engineering and Material Science at Michigan State University.

TABLE OF CONTENTS

LIST OF TABLES

LIST OF FIGURES

KEY TO SYMBOLS

A .....radius of active sites / nm

c.....concentration of bulk intermediate / molecules nm^{-3}

c_s .....concentration of surface intermediate / molecules nm^{-2}

$C_D{}^J$ .....flux control coefficient for diffusivity

$C_E{}^J$.....flux control coefficient for enzyme concentration

$C_{k_1}{}^J$ .....flux control coefficient for rate constant of first active site

$C_{k_2}{}^J$ .....flux control coefficient for rate constant at second active site

d .....distance between active sites / nm

D.....diffusion coefficient / $nm^2\ s^{-1}$

Da .....Damköhler number

D_s .....surface diffusion coefficient / $nm^2\ s^{-1}$

e .....elementary charge / C

E .....enzyme concentration / mol nm^{-3}

F .....Faraday's Constant / C mol^{-1}

I .....ionic strength / M

J .....metabolic flux / mol $nm^{-2}\ s^{-1}$

k_{ads} .....first order rate constant for adsorption / molecules s^{-1}

k_B .....Boltzmann constant / molecules s^{-1}

k_1.....zeroth order rate constant for first active site / molecules $nm^{-2}\ s^{-1}$

k_2 .....first order rate constant for second active site / molecules s^{-1}

k_2' .....first order rate constant for second active site for adsorption model / s^{-1}

K_a .....adsorption coefficient

n .....number of surface charges

N .....diffusive flux / molecules nm^{-2} s^{-1}

N_a .....Avogadro constant / mol^{-1}

r_{ads} .....rate of adsorption / molecules nm^{-2} s^{-1}

r_{cs} .....rate of c_s production / molecules nm^{-2} s^{-1}

r_1 .....rate of intermediate production / molecules nm^{-2} s^{-1}

r_2 .....rate of intermediate consumption / molecules nm^{-2} s^{-1}

R .....gas constant / J K^{-1} mol^{-1}

S .....surface area of connecting bridge / nm^2

T .....temperature / K

v .....external velocity / nm s^{-1}

v_E .....reaction rate of enzyme / mol nm^{-2} s^{-1}

y .....yield of intermediate at second active site

Z .....formal charge of intermediate

ε_r .....relative permittivity

ε_0 .....vacuum permittivity / F m^{-1}

κ^{-1} .....debye length / nm

ρ_s .....surface charge density / e nm^{-2}

ρ_v .....space charge density / C nm^{-3}

ϕ .....potential / V

CHAPTER 1

INTRODUCTION

Nature has developed highly efficient catalytic pathways that accomplish multistep reactions with high selectivity and activity at moderate temperatures and pressures. Examples these multi-enzyme pathways include The Krebs Cycle[1], glycolysis[2], and The Calvin Cycle[2]. These pathways involve a sequence of enzyme-catalyzed reactions whose efficiency is often enhanced by substrate channeling, wherein the product of an enzymatic step is transported to a second enzyme to act as a substrate without relying purely on diffusion. Substrate channeling may decrease the time required for transport between active sites, but also protects the intermediate from escaping into the bulk where it could be recruited to other reactions occurring in the cell.[3,4,5,6]

Nature has developed several methods of substrate channeling to improve intermediate transport to the second reaction active site (Figure 1). One example was discovered from the crystal structure of tryptophan synthase in 1988[7]. Tryptophan synthase is an enzyme complex comprising an α and β active site. The crystal structure of tryptophan synthase revealed a 25 Å tunnel connecting the two active sites. The uncharged intermediate, indole, is produced at the α-site and travels to the β-site via the tunnel, which provides geometric confinement that prevents escape of the indole molecule to the bulk solvent. This is a unique example as most enzyme complexes in nature do not form these tunnels.[7]

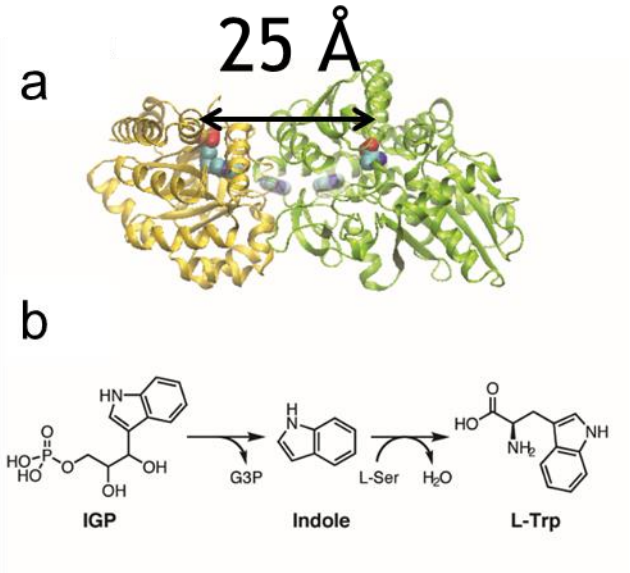

Figure 1. **Substrate channeling in the enzyme complex tryptophan synthase.**[16,7] a). Crystal structure of the enzyme. The active sites are separated by a distance of 25 Å. b). Indole 3-glycerol phosphate (IGP) reacts at the first active site to form the intermediate, indole. The indole is then channeled to the second active site via a molecular tunnel where it reacts to form L-tryptophan.

An alternative mechanism for substrate channeling is found in the bifunctional enzyme dihydrofolate reductase-thymidylate synthase (DHFR-TS), shown in Figure 2. The channeled intermediate is dihydrofolate which carries a formal charge of -2. The active sites are separated by a distance of 40 Å, with no connecting tunnel.[8,9] In 1994, Knighton et al. observed that the protein surface spanning the two active sites contains positively charged residues. It was hypothesized that the negatively charged intermediate, dihydrofolate, electrostatically interacts

with the positively charged surface, channeling dihydrofolate to the second active site.[10]

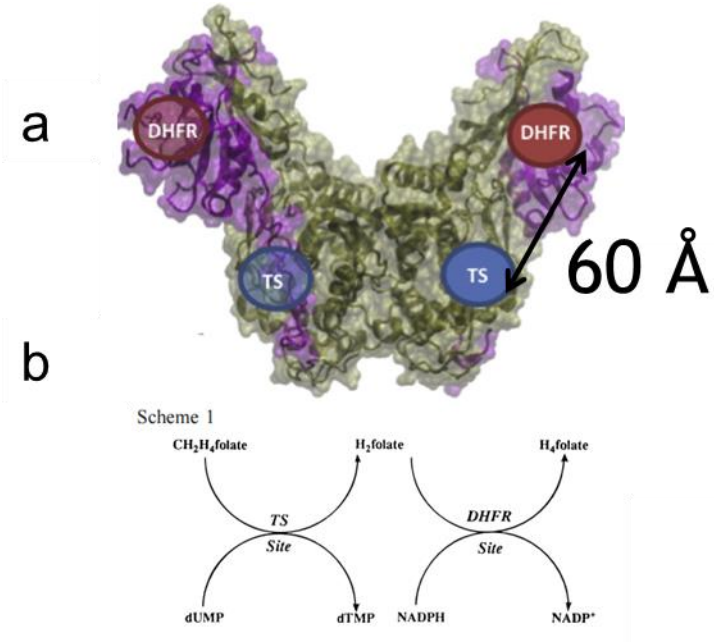

Figure 2. **Substrate channeling in the enzyme complex dihydrofolate reductase-thymidylate synthase.**[10,16] a). Crystal structure of the enzyme. The active sites are separated by a distance of 60 Á. b). Methylenetetrahydrofolate reacts at the first active site to form the intermediate, dihydrofolate. The indole is then channeled to the second active site by interacting with positively charged residues to react and form tetrahydrofolate.

This idea has been supported by simulation work and is thought to be a widely utilized method of substrate channeling as most natural intermediates contain a formal charge.[11,12] Another well-studied enzyme complex is malate dehydrogenase (MD)-citrate synthase (CS), shown in Figure 3. Electrostatic interactions occur between the negatively charged intermediate, oxaloacetate, and a positive charged patch on the enzyme, channeling the intermediate to the second active site.[13,14] The concept of improving substrate channeling to enhance enzymatic

activity has been utilized in organizing catalyst cascades[15].

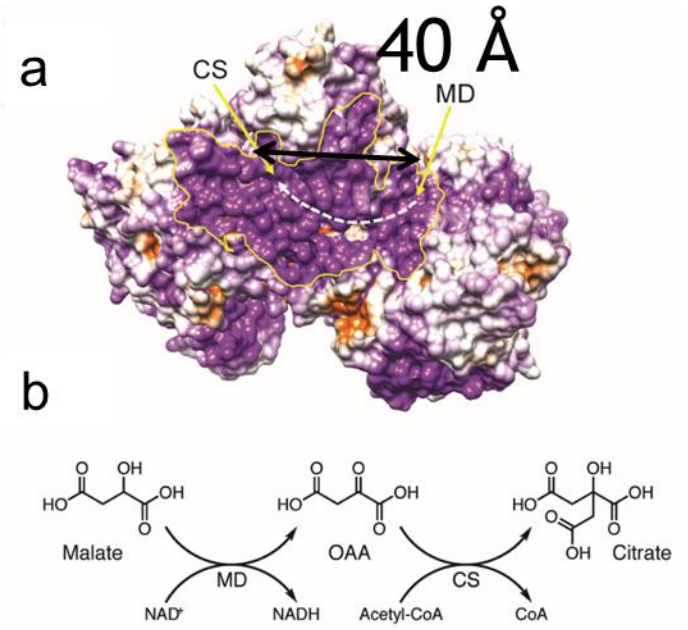

Figure 3. **Substrate channeling in the enzyme complex malate dehydrogenase (MD)-citrate synthase (CS).**[13,16] a). Crystal structure of the enzyme. The active sites are separated by a distance of 40 Å. The positively charged protein surface connecting the active sites is highlighted in yellow. b). Malate is oxidized to form oxaloacetate (OAA) at the first active site. OAA is then channeled to the second active sites through electrostatic interactions where it reacts to form citrate.

The main challenge to overcome in engineering enzymatic or catalytic complexes is diffusion. Wheeldon *et al.* discuss the limits of substrate channeling by simple proximal placement of neighboring active sites. At typical enzyme turnover rate, ~ 10 s^{-1}, and diffusivity 10^3 μm^2 s^{-1} active sites must be placed within 10 nm of each other to maintain intermediate concentrations significantly above bulk values.[16] Tethering enzymes to a molecular scaffold is one way to control the proximity between the active sites. Previous literature has shown the advantages of spatial organization of enzyme cascades using engineered scaffolds.[17] Organizing successive enzymes in a cascade and directly controlling the proximity between them can enhance the activity of the overall cascade.[18] DNA has been utilized as a scaffold for enzyme

immobilization as the distance between enzymes can be precisely controlled and many molecules have been shown to adsorb the surface of DNA.[19,20,21] Wheeldon *et al*. showed enhancement of enzymatic activity with the addition of a DNA scaffold that allowed for substrate adsorption.[19] Substrate-DNA binding energies ranged from 8-23 kJ mol^{-1}.

Elcock *et al.* simulated substrate channeling for the enzyme complex DHFR-TS using Brownian Dynamics.[11] High yields were obtained using a negatively charged intermediate and positively charged bridge connecting the active sites (Figure 4).

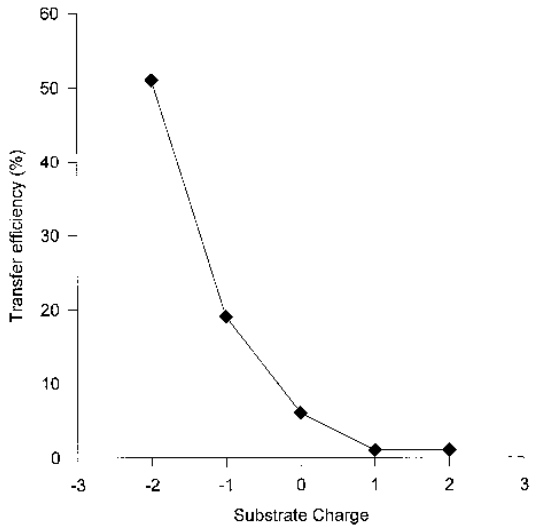

Figure 4. **Electrostatic channeling in DHFR-TS.**[11] Dependence of the transfer efficiency (percent yield) on the substrate charge. Transfer efficiency is maximized when the substrate is oppositely charged of the positive protein bridge connecting the active sites. Like charges cause the intermediate to be repelled, lowering the transfer efficiency.

This work proved the importance of electrostatic interactions for the system. Eun *et al.* modeled a system where charged mediators were placed between active sites.[22] The charged mediators facilitated transport of the intermediate to the second active site. As the number of mediators increases, the yield at the second active site increases. This work shows how proximity limitations can be overcome using charged surfaces to improve substrate channeling through

intermediate migration. The effects of enzymatic rate constants and intermediate surface adsorption were not considered. Idan *et al*. modeled substrate channeling between two tethered enzymes, glucose oxidase (GOx) and horseradish peroxidase (HRP).[23] While this work supported the importance of proximity between active sites, it also showed that having a surface for intermediate adsorption and diffusion can increase substrate channeling (Figure 5).

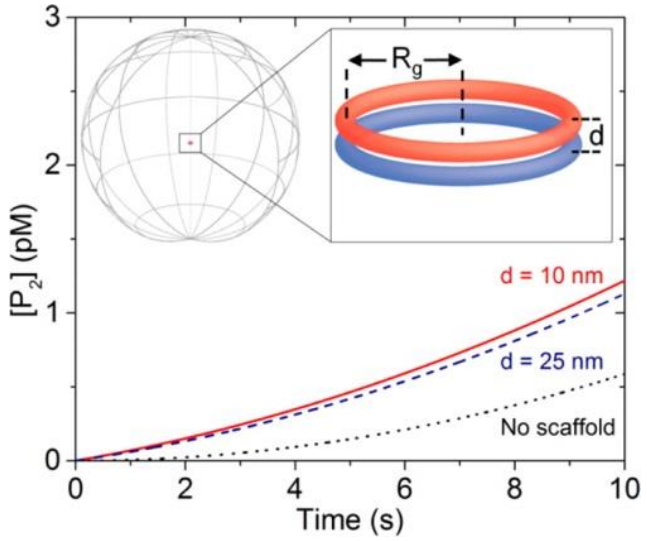

Figure 5. **Reaction diffusion simulation for GOx-HRP pairs on a folded scaffold.**[17] The rate of product formation increases with the addition of the scaffold.

Here we describe a steady-state continuum model for substrate channeling between two active sites that accounts for channeling by proximity, surface adsorption, and electrostatic interactions (Figure 6). Kinetics at both active sites are explicitly included to allow determination of the kinetic rates necessary to achieve efficient channeling.

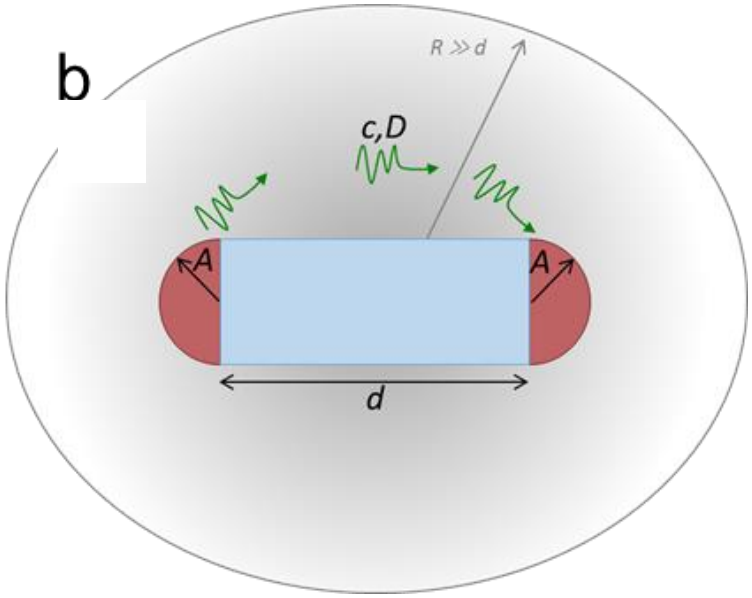

Figure 6. **Steady state continuum model.** The intermediate is produced at the first active site and can be consumed at the second active site or diffuse out of the model at the domain edge. The connecting bridge can be utilized to facilitate substrate channeling.

A zero-concentration boundary condition at the domain edge eliminates any contribution of bulk intermediate to yield at the second active site. The effects of transport properties such as the diffusion coefficient, kinetic rate constants and potential field are quantified by utilizing metabolic control analysis (MCA). MCA has traditionally been used in purely kinetic systems and this paper proposes incorporating transport into this calculation.[24,25] This approach reveals the kinetic and transport regimes in which these channeling mechanisms can be effective.

CHAPTER 2

BASE MODEL

Model Description

A continuum model, shown in Figure 7, comprises two spherical active sites of radius A separated by distance d and centered in an ellipsoidal domain of width R and length $R + d$. A substrate reacts at the first active site to produce an intermediate of concentration c which is transported to the second active site. A "bridge" surface connects the two active sites, allowing for surface transport and/or surface charge, depending on the channeling mechanism employed. In order to focus on the intermediate, zeroth order kinetics are assumed at the first active site:

$$r_1 = k_1 \quad [1]$$

where $k_1$is a zeroth order rate constant. The kinetics at the second active site are assumed to be first order in intermediate concentration:

$$r_2 = k_2 \mathrm{c} \quad [2]$$

with k_2 defined as the first order rate constant. Mass transport is defined by a modified Nernst-Planck Equation[27]:

$$N_\mathrm{i} = \frac{z_\mathrm{i} D_\mathrm{i} F}{RT} c_\mathrm{i} \nabla\phi - D\nabla c_\mathrm{i} \quad [3]$$

with N_i defined as the flux of intermediate, z the formal charge of the intermediate, D the diffusion coefficient, F Faraday's Constant, R gas law constant, T temperature, ϕ potential, and v velocity. The surface connecting the two active sites is assumed to allow no normal flux. Convective flux was neglected in this model. In order to focus on substrate channeling between

adjacent active sites, the outer domain edge cannot have a no-flux boundary condition. Instead the boundary conditions are listed below.

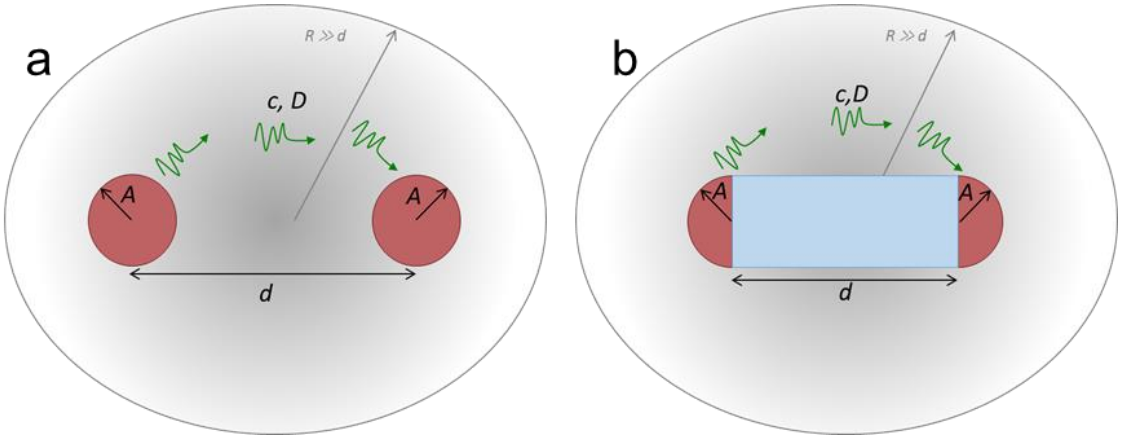

Figure 7. **General schematics for the base model.** a). A base case with no connecting bridge is modeled for comparison b). The bridge connecting the active sites can act as a physical barrier.

The outer domain edge was set to have a zero concentration. In this context, the material balance in the absence of bulk reaction was solved:

$$\nabla \cdot N = 0 \qquad [4]$$

At the active sites, the material balance of flux is equal to the reaction rates. The flux of intermediate perpendicular to the connecting bridge is zero. With this model, the effects of rate constants, diffusivity, and geometry were explored, with base-case parameter values given in Table 1. The above equations were solved numerically in two-dimensional, axisymmetric geometry using COMSOL Multiphysics®.

Table 1. Parameter Values for Base Model

Parameter	Value
***d*, distance between active sites / nm**	5
***R*, radius of model domain / nm**	20
***A*, radius of active sites / nm**	1
k_1, zeroth order rate constant at first active site / molecules nm^{-2} s^{-1}	10
k_2, first order rate constant at second active site / nm s^{-1}	10^{12}
***D*, diffusion coefficient / nm^2 s^{-1}**	10^9
T, temperature / K	298

Yield

Percent yield is important to calculate to get an idea of how efficient the system is at transporting the intermediate to the second active site. In the system, the intermediate can either be transported to the second active site or diffuse out the model. The percent yield is defined as the flow of intermediate to the second active sites divided by the flow of intermediate produced at the first active site. This can be simplified to:

$$\text{Percent Yield} = \frac{r_2}{r_1} * 100 \qquad [5]$$

Mass transfer limited case

In the model, the yield of intermediate at the second active site is limited by two phenomena: kinetic reaction rates, and the mass transport between active sites. To study the mass transfer limited case, the kinetics of the system can be assumed to be perfect. This occurs at very high values of the rate constant at the second active site, with $k_2 = 10^{12}$nm s^{-1}.

Nondimensionalization

Nondimensionalization is a technique widely utilized for the partial or full removal of units from an equation. This allows for comparisons to different systems independent of the physical scale of the system. The Damköhler number is a dimensionless number that relates the time constant for reaction rates to the time constant for mass transport occurring in the system. It can be defined as:

$$\mathbf{Da} = k_2 A/D \qquad [6]$$

Results

The figure of merit for transport efficiency in this two-site system is yield of product at the second active site. At steady state, the intermediate is either converted to product or diffuses to the domain edge. Assuming fast kinetics at both sites, the yield may be calculated using the relative flux at site 2 compared to site 1. When kinetic limitations are considered, yield is calculated as the ratio of reaction rates (molecules s^{-1}).

Mass Transfer Limited Case (Infinite Kinetics)

The mass-transfer limited yield provides an upper limit for the yield when kinetic limitations are considered. For mass-transfer limited conditions, we set the concentration of intermediate at site 2 to zero. Because the bridge surface can impede direct diffusion, an alternative geometry without the bridge was also considered, as shown in Fig. 8b, which can be compared to Fig. 1a. Figure 8a shows a concentration gradient profile. The intermediate concentration is highest at the first active site, and rapidly decreases moving away from the first active site.

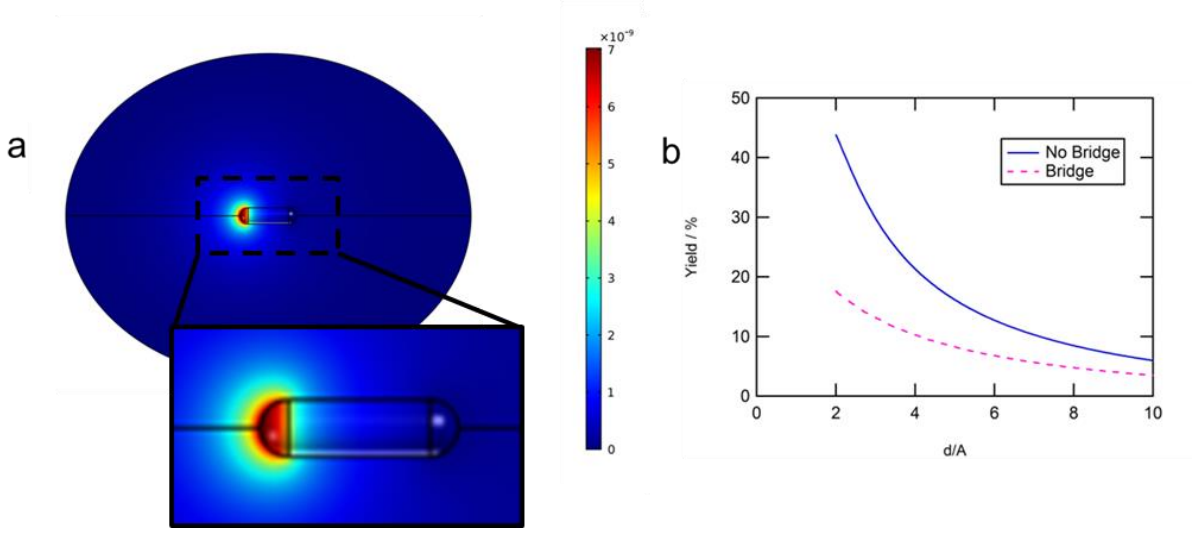

Figure 8. **Yield under mass-transfer limited conditions.** a) Concentration profile, the units of concentration are molecules nm^{-3}. b) Comparison of the yield versus distance between active sites between the bridge and no bridge data. All other parameter values listed in Table 1.[30]

In Figure 8b percent yield is plotted varying spacing, d, normalized to the site radius, A, for cases where the bridge is absent and included. Here, the bridge does not facilitate transport, and instead acts as a barrier for intermediate transport to the second active site, decreasing the overall yield. With no bridge present, and at $d/A = 2$, corresponding to minimal distance between the spherical active sites, the yield approaches 45%, corresponding to the maximum value attainable from channeling by proximity alone. As the distance between active sites increases, the intermediate is more likely to escape into the bulk solution, decreasing the overall yield at the second active site. Introducing the bridge increases the diffusive path length between active sites, decreasing the yield approximately twofold.

Kinetically Limited Case

Kinetic limitations reduce yield compared to the mass-transfer limited case. In Figure 9, yield is plotted for various active site spacing, d, with respect to the surface rate constant k_2, with

and without the bridge. Equivalently, the data is also plotted versus the Damköhler number, **Da**, which relates the time constant for the reaction at site 2 to the time constant for mass transport. Fig. 9a demonstrates that values of the rate constant, k_2, greater than 10^7 nm s^{-1} are required to achieve significant yield. Relatively few catalysts are capable of such turnover rates.[16] Values of k_2 greater than 10^{10} nm s^{-1} are required to reach the yield plateau, equivalent to the mass-transfer limited cases of Fig. 8. Fig. 9b demonstrates that the transition from kinetic limitation to mass transfer limitation occurs at **Da**=1, corresponding to $k_2=10^9$ nm s^{-1}.

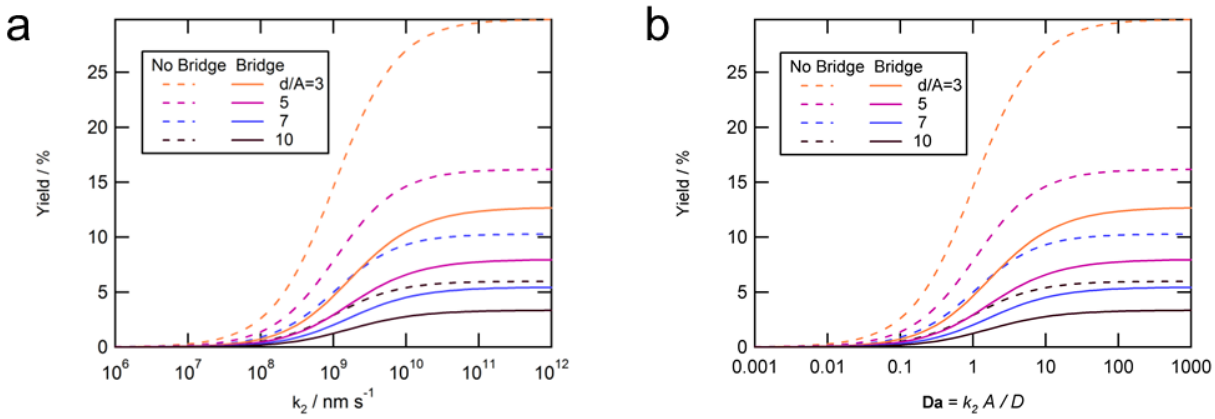

Figure 9. **Yield under kinetically limited conditions.**[30] a. Comparison of the yield versus k_2.Large values of k_2 are needed to see a significant yield. b. Dimensionless form, where yield is plotted versus Damkohler number, **Da**. All other parameter values listed in Table 1.

Discussion

The distance between active sites as shown to be important parameter for maximizing the yield of intermediate to the second active site. At distances higher than 5 nm, the yield rapidly decreased to values under 10%. The connecting bridge was shown to be a geometric barrier that limited the yield, when only diffusion was utilized as a mode of transportation. The introduction of kinetics allowed for the determination of rate constants needed for a sufficient yield. Mass

transfer limited conditions (high values of **Da**) were required to obtain moderate yields. This model shows that diffusion alone is an ineffective mode of substrate channeling and that engineering a connecting bridge can cause a decrease in yield.

CHAPTER 3

METABOLIC CONTROL ANALYSIS

Overview

Metabolic Control Analysis (MCA) is a framework that is used to describe metabolic pathways.[28] MCA connects overall system properties of a metabolic system to the properties of its components. An example of this is how flux will change in response to a change in a parameter such as enzyme concentration. If the system is linearized at steady state, the degree of control of these parameter changes can be quantified by calculating flux control coefficients. The FCC for enzyme concentration is defined below:

$$C_{\mathrm{E}}{}^{J} = \frac{E}{J}\frac{dJ}{dE} \qquad [7]$$

where *C*, *E*, J represent a flux control coefficient, enzymatic concentration and metabolic flux respectively. In the theory, the sum of the FCCs for a given flux should sum to one.

$$\sum_{\mathrm{i}} C_{\mathrm{i}}{}^{J} = 1 \qquad [8]$$

This is called the summation theorem and it shows that FCCs are system properties. Individual parameters, such as enzyme concentration, share control of the flux. If a FCC is equal to one, then that the particular FCC parameter is considered rate-limiting. As well as FCCs, MCA introduces the elasticity coefficients. Unlike FCCs, elasticity coefficients are not properties of the entire system, but of the individual enzyme. The elasticity coefficient is defined below:

$$\varepsilon_{S_c}^{\ E} = \frac{S_c}{v_E}\frac{dv_E}{dS_c} \quad [9]$$

where ε, S, v represent a elasticity coefficient, substrate concentration, and reaction rate of the enzyme respectively The connectivity theorem states that sum of the elasticity coefficients multiplied by the FCCs should sum to zero. This provides an understanding of how FCCs are affected by the kinetics of the enzymes. MCA has traditionally been applied to purely kinetic systems, but for this research it can be applied to a system that also has transport. FCCs for both kinetic and transport can be calculated in order to determine the degree of control that parameter has on the overall flux of the model. For example, the FCC for diffusion is defined below:

$$C_{D_i}^{\ J} = \frac{D_i}{J}\frac{dJ}{dD_i} \quad [10]$$

Parameters of the model can be varied to determine the sensitivity of the flux and the FCC. This will help understand the efficiency of a system that varies with geometry, spacing, rate constants and diffusivity. MCA can be used to evaluate the overall efficiency of the two models that can be developed.

Results

The impact of both the mass transport and kinetic parameters are quantified by calculating flux control coefficient for the kinetic and mass transport parameters, shown in Figure 10. For all values of **Da**, the flux control coefficient C_D^J is negative, meaning that increased diffusivity decreases flux and yield. Only under mass transfer limited conditions at high values of **Da** does C_D^J approach zero. The kinetic FCC for site 2, $C_{k_2}^J$, is equal and opposite to C_D^J, and $C_{k_1}^J$ is unity, reflecting the direct control of the zeroth order rate constant, k_1, on the

overall intermediate flux. The sum of these flux control coefficients is one, obeying the summation theory.

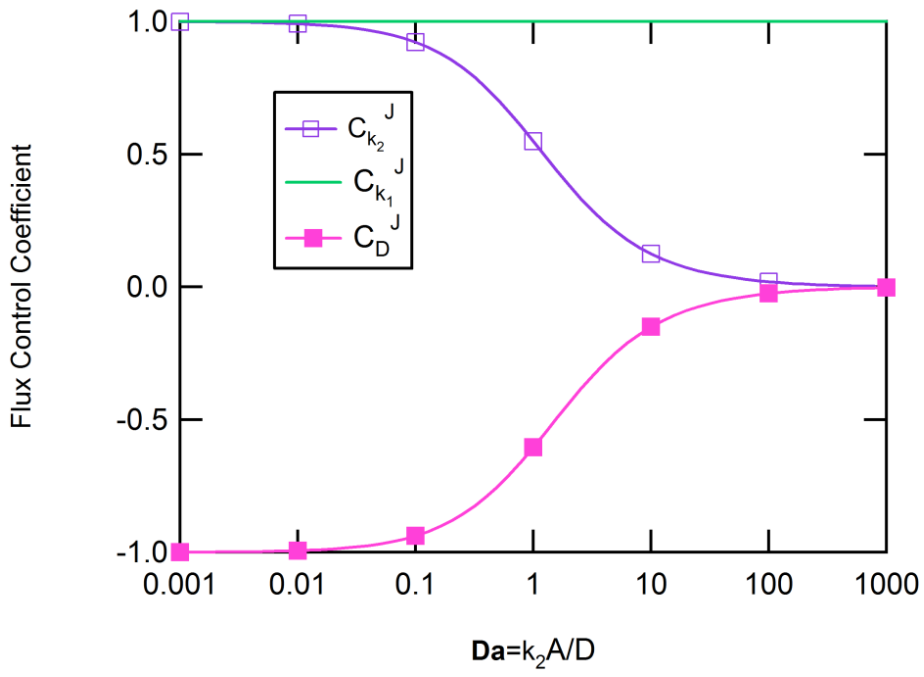

Figure 10. **Plot of flux control coefficients for k_1, k_2, and D.**[30] At low values of **Da** the rate constant for k_2 is rate controlling. k_1 is always rate controlling, while D has a negative contribution to the flux of intermediate to the second active site. Parameters listed in Table 1.

Discussion

Flux control coefficients allow for the quantification of the effect systemic properties have on the flux of intermediate to the second active site. The rate constant at the first active site, k_1, was found to be rate controlling at all values of **Da**. Increasing the flux of intermediate into the model causes a subsequent increase of the flux of intermediate to the second active site. Increasing the diffusivity has a negative impact as the intermediate rapidly diffused to the domain edge. The rate constant at the second active site, k_2 was found to be rate controlling at

low values of **Da**, as the low kinetic activity limited the flux of intermediate to the second active site.

CHAPTER 4

ELECTROSTATIC MODEL

Model Description

Electrostatic interactions between the intermediate and charged surface can facilitate transport (Figure 11).

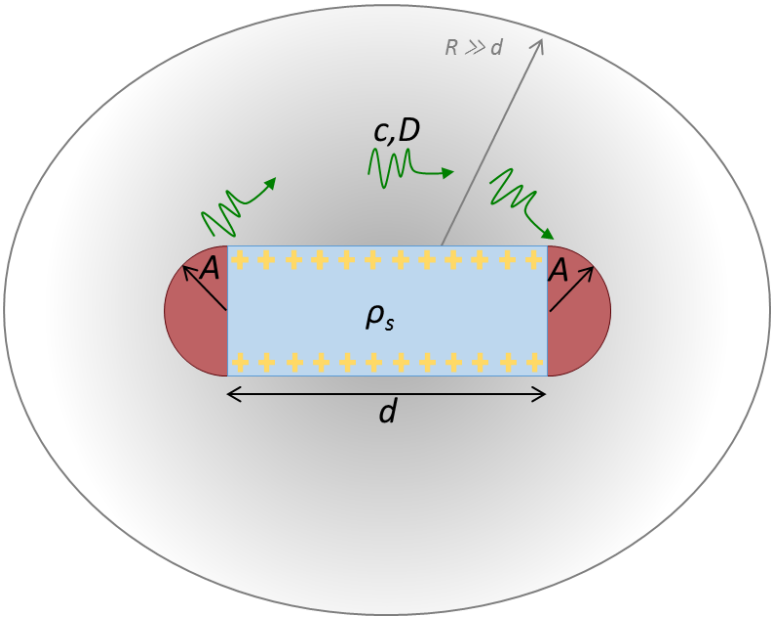

Figure 11. **General schematics for the electrostatic model.** The connecting bridge contains positively charged residues which interacts with the negatively charged intermediate.

The active site-complex may contain charged residues described by a surface charge density.

$$\rho_s = (ne)/S \qquad [11]$$

with n defined as the number of charges, e the elementary charge, and S the surface area of the complex. ρ_s is defined on the connecting bridge, while the active sites remained uncharged. The positively charged surface creates a potential field that enables migration transport. The outer

domain edge has a potential of 0 V. The potential field is given by the Poisson Boltzmann equation[29]:

$$\nabla^2\phi = \left(\frac{z_i e n}{\varepsilon_r \varepsilon_0}\right) \exp\left[\frac{ze\phi}{k_B T}\right] \quad [12]$$

with ε_r defined as the relative permittivity, ε_0 the vacuum permittivity, and k_B the Boltzmann constant. This non-linear equation can be simplified by considering only dilute solutions where the interionic interactions are small, $ze\phi \ll k_B T$. Linear expansion of the exponential combined with assumption of electroneutrality yields

$$\varepsilon_r \varepsilon_0 \nabla^2\phi = \rho_v \quad [13]$$

with ρ_v defined as the space charge density. The space charge density is

$$\rho_v = \frac{1}{\kappa^2} \varepsilon_r \varepsilon_0 \phi \quad [14]$$

Near solid-liquid interfaces, potential varies within the electrical double layer whose width is defined by the ionic-strength dependent Debye length

$$\kappa^{-1} = \left(\frac{\varepsilon_r \varepsilon_0 k_B T}{2 N_a e^2 I}\right)^{1/2} \quad [15]$$

where *I* is the ionic strength in units of M, and N_a is Avogadro's number. Substituting in the debye length the resulting governing equation for the potential field, ϕ, is:

$$\varepsilon_r \varepsilon_0 \nabla^2\phi = -\frac{1}{\kappa^2} \varepsilon_r \varepsilon_0 \phi \quad [16]$$

The potential field, ϕ, within the model can therefore be calculated as a function of ionic strength, I, and surface charge ρ_s. The potential gradient, $\nabla\phi$ controls the migration term of Eq. 3. The flux of intermediate perpendicular to the surface is zero.

Table 2. Parameter Values for Electrostatic Model

Parameter	Value
I, Ionic Strength / M	10^{-3}
ρ_s, surface charge density / e nm^{-2}	0.5
Z, intermediate charge	-2
ε_r, relative permittivity	80

Results

The presence of charged surfaces induces an electrostatic field, which in turns leads to ion accumulation in a double layer that controls charge and potential distributions in solution. The double layer thickness, approximated by the Debye length, is significant compared to the dimensions of this model and depends on the solution ionic strength. The electrical potential field is plotted in Figure 12, taken at a plane halfway between the active sites. The double layer thickness increases from 2.5 to 10 nm as ionic strength decreases. Kinetics are added into the model to understand the contributions of electrostatic interactions. (Figure 13a). When the number of charges per nm^2 is high, and the intermediate is oppositely charged, yield becomes significant for **Da** $\ll 1$, in fact as low as 10^{-7}. The effects of substrate charge and surface charge on the yield of intermediate at the second active site is shown in Figure 13b. Under these conditions, a substrate charge of -1 to -2 is more than enough to dramatically increase yield.

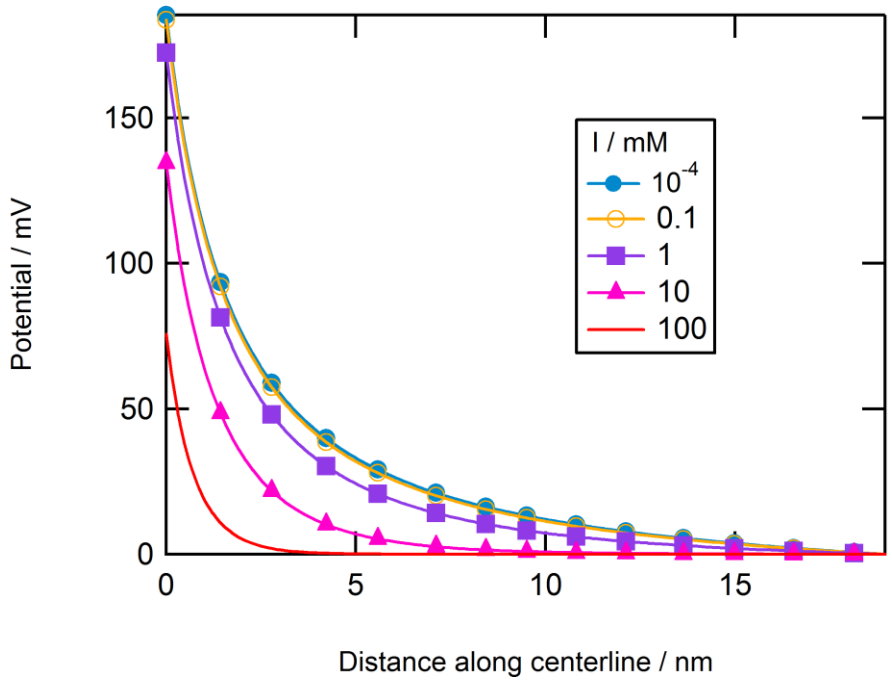

Figure 12. **Potential along the centerline at increasing ionic strength.** Increasing the ionic strength decreases the distance the electrostatic effects are felt in the model. Parameter values given in Tables 1-2.[31]

The effect of ionic strength on the yield of intermediate to the second active site is shown in Figure 13c. Depending on surface charge, ionic strength as high as 10^{-3} to 10^{-2} M is sufficiently low to achieve significant yield.

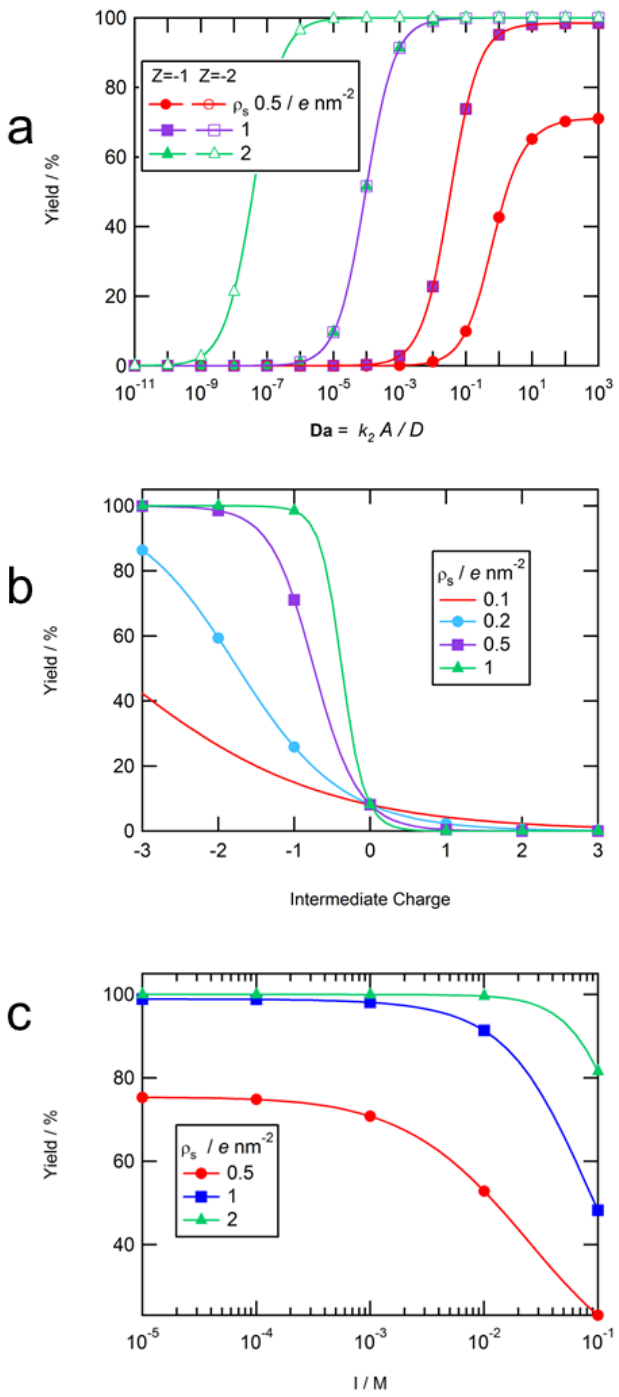

Figure 13. **Electrostatic interaction plots.**[31] a). Yield versus **Da** at varying ρ_s and substrate Z combinations. At ideal combinations of charges, the **Da** required to obtain significant yields, decreases. Other parameter values given in Table 1. b). Yield versus substrate charge at varying ρ_s. The yield decreases the substrate charge becomes more positive due to like charges repelling. Other parameter values given in Table 1. c). Yield versus the ionic strength at varying distances between active sites. As the ionic strength increases initially, the yield remains constant until high enough ionic strengths cause the yield to decrease. Other parameter values given in Table 1-2.

Discussion

Electrostatic interaction was found to be an efficient mode of substrate channeling. The negatively charged intermediate interacted with the positively charged bridge to facilitate transport. The product of ρ_s and Z was found to be the important parameter affecting yield. As the product increased, the yield reached values close to 100% in the mass transfer limited region. The transition from the kinetically limited region to mass transfer limited (measured by **Da**) shifted to lower values with the addition of electrostatic interactions. This means higher yields can be reached at lower, and more realistic values of rate constants. The effects of ionic strength were also measured. High values of I (over 10 mM) was found to have a negative effect on yield. The decrease in yield is due to the decrease in the debye length, or the length at which electrostatics persist in the solution. At low values of I, which are common in dilute solutions, the yield remained constant with ionic strength. Electrostatic interactions proved to be an efficient mode of transport for substrate channeling with high yields (over 95%) observed at lower values of the **Da** number.

CHAPTER 5

SURFACE ADSORPTION MODEL

Model Description

Surface transport of intermediates was explored by considering the generation of a surface intermediate, c_s:

$$r_{cs} = k_1 \quad [17]$$

The surface intermediate is in equilibrium with the bulk intermediate, *c*, with an adsorption coefficient K_a. The rate of reversible adsorption is described by

$$r_{ads} = k_{ads}\left(c - \frac{c_s}{K_a}\right) \quad [18]$$

with k_{ads} being defined as the rate constant for adsorption. The surface intermediate, c_s, can diffuse across the surface to the second active site, with a surface diffusivity, D_s. The resulting material balance for the surface species is therefore

$$c_s = K_a c \quad [19]$$

The surface intermediate is consumed at the second active site via a first-order reaction

$$r_2 = k_2' c_s \quad [20]$$

with $k_2{}'$ defined as the first order surface rate constant at the second active site. Two models for adsorption are explored. Model one is where the surface species can diffuse across the entire

complex, and the second where diffusion is limited to the connecting bridge (Figure 14).

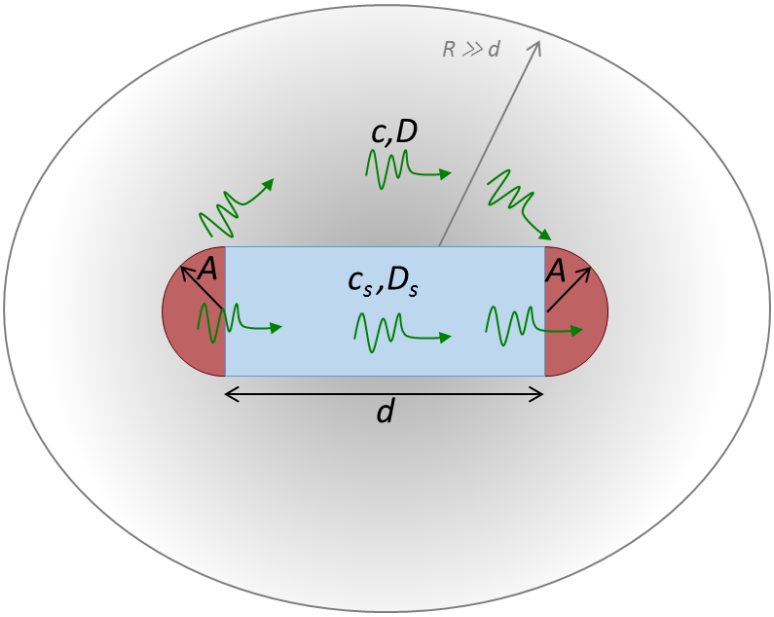

Figure 14. **General schematic for the surface adsorption model.** Surface diffusion can be limited to the connecting bridge (left) or allowed on the entire surface.

The parameters for this model are summarized in Table 3.

Table 3. Parameter Values for Surface Adsorption Model

Parameter	Value
k_2', first order rate constant for the second active site / s^{-1}	10^9
k_{ads}, first order rate constant for adsorption / nm s^{-1}	10^{14}
K_a, adsorption coefficient / nm	1000
D_s, surface diffusion coefficient / nm^2 s^{-1}	10^9

Nondimensionalization

For the surface adsorption model, the Damköhler number requires the addition of the adsorption coefficient.

$$\mathbf{Da} = k_2' A K_\mathrm{a} / D \qquad [21]$$

Results

When surface adsorption is considered, the definition of the Damköhler number, **Da**, changes by the addition of the adsorption coefficient, K_a (Figure 15b). Results for the two models of surface adsorption are shown. Because the intermediate concentrations considered here are low (~10^{-6} molecules/nm3) the resulting surface concentration is much less than a monolayer. Varying K_a leads to shifts in the rate constant, k_2', needed for significant yield, but does not affect the transition value of **Da** or the maximum achievable yield. When the intermediate is allowed to surface-diffuse from the first active site to the second active site directly (Model 1), the yield is significantly higher, at lower kinetic rates, than when the intermediate is required to re-adsorb onto the surface (Model 2). The effects of varying surface diffusivity, D_s, are shown in Figure 9b. Varying D_s does not affect the transition value of **Da**, but does affect the maximum yield. In summary, realistic values of adsorption coefficient, K_a, and surface diffusivity, D_s, are insufficient to lower the kinetic rates required for high yield.

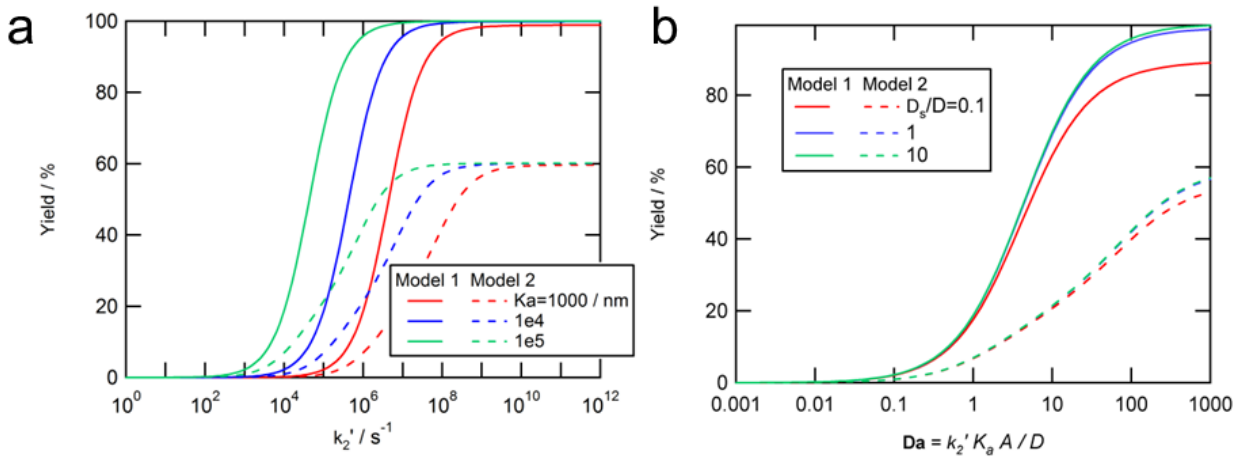

Figure 15. a). **Yield versus k_2' at varying values of K_a.** b).Yield versus **Da** at varying surface diffusivities. Increasing surface diffusivities causes an increase in yield at high **Da**. All other parameters are listed in Tables 1 and 3.[32]

Discussion

The efficiency of surface adsorption was found to be dependent on the model. When surface adsorption and diffusivity was limited to the connecting bridge, the yield plateaued at around 60%. When the intermediate was allowed to diffuse from the first active site to the second active site, the yield approached 100% at high values of **Da**. Surface diffusivity was found to have a minimal effect on the yield. Overall, channeling by surface adsorption was found to be ineffective modes of transport, with high yields only being obtained at high values of the **Da**.

CHAPTER 6

SYNTHESIS

Model Description

With the effects of electrostatic interactions and surface adsorption understood, the models can be combined to attempt to maximize the intermediate transport between active sites. The intermediate was allowed to directly diffuse from the first active site to the second.

Results

The effects of electrostatic interactions and surface adsorption can be considered together to determine their combined effect on intermediate transport and yield. The combined effects are shown in Figures 16. When electrostatic interactions are present, high yields are reached at lower values of **Da**. Whereas surface diffusivity, D_s , directly impacts maximum yield in the absence of electrostatic interactions, very low surface diffusivity is required to reduce maximum yield when electrostatic interactions are present.

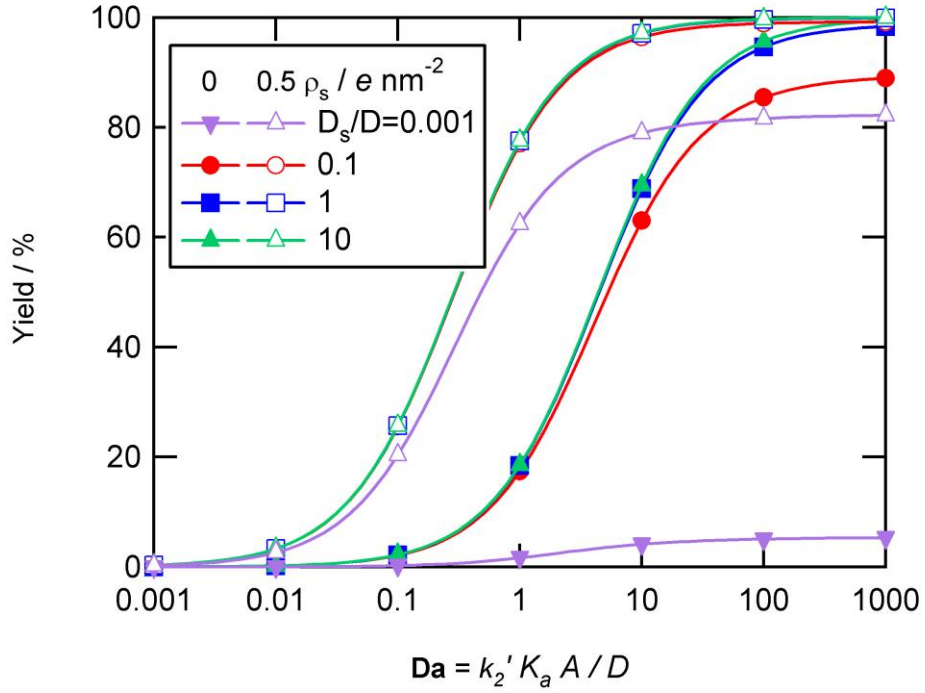

Figure 16. **Yield versus Da at varying values of $D_s$and ρ_s.** The yield increases dramatically with the addition of electrostatics, while increasing the surface diffusivity does not contribute largely to yield. Parameters for this plot are listed in Tables 1-3.[33]

Comparison with experimental results

Experimental results for channeled systems are often reported in terms of transient times, τ, which is the time taken for a reaction to reach steady state. Short transient times are associated with systems that channel efficiently.[8,12] Based on the analysis of Elcock *et al*. the transient time can be calculated by $(1-y)\,A\,/k_2$ where y is the calculated yield.[12] The effects of **Da** on τ for two scenarios are shown in Figure 17. Proximity alone is not an effective mode of substrate channeling, as there is a very small decrease in transient time as **Da** increases. When electrostatic interactions are introduced, however, there is a rapid decrease in transient time as **Da** increases, proving it to be an effective mode of substrate channeling.

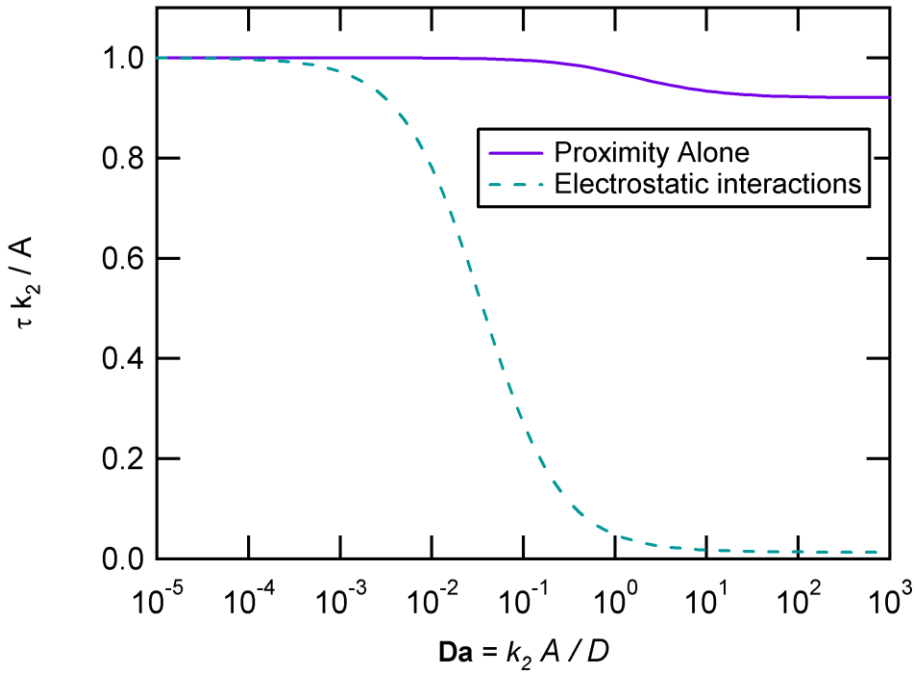

Figure 17. **Transient time versus Da.** Parameter values given in Tables 1 and 2.[32]

Discussion

The combination of surface adsorption and electrostatic interactions produces few benefits. Similar to the surface adsorption model, increasing the diffusivity to higher values has little effect on yield. The shift from kinetic limitations to mass transfer limitations does not shift to lower values of **Da** in the combined model. The addition of electrostatic interactions can also help overcome the negative effects of low surface diffusivity. The maximum yield for systems with low values of diffusivity increases from under 5% to over 80% with the addition of electrostatics.

Calculating transient time allows for a bridge between experimental and model systems. When proximity alone is the main method of substrate channeling, there is a small decrease in

transient time at high values of **Da**. Most enzymatic systems are unable to reach the turnover rates necessary for these values of **Da**. With the addition of electrostatics, the transient time decreases significantly at lower values of **Da** ($\sim 10^{-2}$).

CHAPTER 7

CONCLUSIONS AND FUTURE PERSPECTIVES

In this work, substrate channeling between actives sites was investigated using numerical continuum modeling. The effects of both kinetic reaction rates and mass transport were incorporated. Several different modes of transport were considered including channeling by proximity, electrostatic interactions and surface adsorption. Channeling by proximity alone was found to be an inefficient mode of transport. Maximum yields of ~50% were only obtained at mass transfer conditions (infinite kinetics) and by limiting the distance between active sites to 2 nm. Surface adsorption increased the maximum yield, but required large values of **Da**, which is unobtainable to most enzymatic systems. Electrostatic interactions, however, proved to be an efficient mode of transport with high yields (over 95%) observed at lower values of the Damköhler number. The addition of electrostatic interactions can also help overcome the negative effects of low surface diffusivity. Transient times were also calculated to link experimental and numerical simulations. Electrostatic interactions were found to be an efficient mode of substrate channeling due to the decrease in lag time at lower values of **Da**.

Recognizing that the present modelling approach ignores significant molecular details of specific reacting systems, the results here provide a framework for considering the technical potential of various channeling modes. Knowledge gained from this model could lead to the development of biomolecular-scaffold systems where electrostatic interactions control intermediate transport, and these constructed scaffolds could be incorporated into catalyst cascades. Ongoing work includes modeling geometric confinement through molecular tunnels, such as the one found in the enzyme complex tryptophan synthase. A realistic example of this

could be catalysts present in a tunnel. Preliminary results show this to be a highly efficient mode of channeling.

Through modeling, a solid understanding of the different modes of substrate channeling has been gained. The next step is to develop multi-step catalytic models that can determine the efficiency of an entire system. There are unique challenges that exist in these multi-component systems that could decrease the efficiency of substrate channeling. These technical hurdles could include spatial organization of enzymes, different methods of inhibition, such as product or competitive inhibition, and competing side reactions that could sequester molecules of the pathway. Developing an understanding through modeling of how these problems affect substrate channeling, will help lead to solutions to overcome them and assist in the design of catalytic systems that maximize product yield.

APPENDICES

Appendix A: Intermediate concentration as a function of position derivation

In order to verify the accuracy of the continuum model, a general equation for intermediate concentration can be derived. One-dimensional diffusion is assumed from a symmetrical cylindrical surface. For a cylindrical system:

$$\frac{\partial c}{\partial t} = -D\left[\frac{1}{r^2}\frac{\partial}{\partial r}\left(r^2\frac{\partial c}{\partial r}\right)\right] \quad [22]$$

At steady state, there is no accumulation so the equation simplifies to:

$$0 = -D\left[\frac{1}{r^2}\frac{\partial}{\partial r}\left(r^2\frac{\partial c}{\partial r}\right)\right] \quad [23]$$

Integrating both sides gives:

$$\mathrm{C}_1 = r^2\frac{\partial c}{\partial r} \quad [24]$$

with C_1 representing a constant of integration. A second integration, and the boundary condition $c = 0$ at $r = r_2$, leads to the equation:

$$\mathrm{c} = \frac{\mathrm{C}_1}{r_2} - \frac{\mathrm{C}_1}{\mathrm{r}} \quad [25]$$

Using equation 24, and the boundary condition at $r = r_1$:

:

$$\mathrm{k}_1 = -\mathrm{D}\frac{\partial c}{\partial r} \quad [26]$$

The constant of integration can be solved for and the final equation for concentration is obtained:

$$\mathrm{c} = \frac{\mathrm{k}_1}{D}{r_1}^2\left(\frac{1}{r_1} - \frac{1}{r_2}\right) \quad [27]$$

The relationship between surface intermediate and bulk intermediate can be utilized to solve for the surface concentration:

$$c_s = \frac{k_1}{D} K_a {r_1}^2 \left(\frac{1}{r_1} - \frac{1}{r_2}\right) \quad [28]$$

By plugging in the appropriate values for the parameters (K_a, k_1 and D listed in Tables 1 and 3) and $r_1 = 1$ nm, $r_1 = 20$ nm, the surface concentration can be solved for and the value is $9.5*10^{-6}$ molecules nm^{-2}.

Appendix B: Flux control coefficient summation theory[26]

In a linear pathway of enzymes, the reaction mechanism can be written as:

$$S_1 + E_1 \rightarrow S_1E_1 \rightarrow P_1 + E_2 \rightarrow P_1E_2 \rightarrow P_2 + E_3 \rightarrow P_2E_3 \quad [29]$$

with the product of the first reaction acting as a substrate to the next reaction. The flux to the final enzyme, E_3, can be measured at steady state. All the individual enzyme pools will also be at steady state because the net rates of formation and consumption are equal. If the concentration of enzymes are all equally changed by a fractional amount, α:

$$\frac{\partial E_i}{E_i} = \alpha \quad [30]$$

The balance of all the rates of the system would remain the same, but the fractional change in overall flux, which is simply a sum of the individual changes, would be:

$$\frac{\partial J}{J} = \sum \frac{\partial J_i}{J_i} = \alpha \quad [31]$$

The definition of a flux control coefficient is the fractional change in flux due to the fractional change in a system property. The flux control coefficient for an individual enzyme concentration can be written as:

$$\left(\frac{\partial J_i}{J_i}\right) / \frac{\partial E_i}{E_i} = C_i^J \quad [32]$$

For each enzyme, a flux control coefficient can be calculated. Using equation 29:

$$\left(\frac{\partial J_i}{J_i}\right) = \alpha C_i^J \quad [33]$$

The summation (equation 30) gives:

$$\frac{\partial J}{J} = \sum_i \left(\frac{\partial J_i}{J_i}\right) = \alpha \sum_i C_i^J \quad [34]$$

Using equation 30, this simplifies to the summation theory:

$$\sum_{\mathrm{i}} C_{\mathrm{i}}{}^{J} = 1 \qquad [35]$$

REFERENCES

REFERENCES

1. Wu, F. & Minteer, S. Krebs Cycle Metabolon: Structural Evidence of Substrate Channeling Revealed by Cross-Linking and Mass Spectrometry. *Angew. Chemie Int. Ed.* **54,** 1851–1854 (2015). DOI: 10.1002/anie.201409336

2. Berg, J. M., Tymoczko, J. L. & Stryer, L. Biochemistry. (2002).

3. Miles, E. W., Rhee, S. & Davies, D. R. The Molecular Basis of Substrate Channeling. *J. Biol. Chem.* **274,** 12193–12197 (1999). DOI: 10.1074/jbc.274.18.12193

4. Winkel, B. S. J. Metabolic channeling in plants. *Annu. Rev. Plant Biol.* **55,** 85–107 (2004). DOI: 10.1146/annurev.arplant.55.031903.141714

5. Srere, P. A. The metabolon. *Trends Biochem. Sci.* **10,** 109–110 (1985). DOI: 10.1016/0968-0004(85)90266-X

6. Srere, P. A. Complexes of sequential metabolic enzymes. *Annu. Rev. Biochem.* **56,** 89–124 (1987). DOI: 10.1146/annurev.biochem.56.1.89

7. Hyde, C. C., Ahmed, S. a., Padlan, E. a., Miles, E. W. & Davies, D. R. Three-dimensional structure of the tryptophan synthase α2β2 multienzyme complex from Salmonella typhimurium. *J. Biol. Chem.* **263,** 17857–71 (1988). DOI: 10.1074/jbc.X113.463331

8. Trujillo, M., Donald, R. G. K., Roos, D. S., Greene, P. J. & Santi, D. V. Heterologous expression and characterization of the bifunctional dihydrofolate reductase-thymidylate synthase enzyme of Toxoplasma gondii. *Biochemistry* **35,** 6366–6374 (1996). DOI: 10.1021/bi952923q

9. Meek, T. D., Garvey, E. P. & Santi, D. V. Purification and characterization of the bifunctional thymidylate synthetase-dihydrofolate reductase from methotrexate-resistant Leishmania tropica. *Biochemistry* **24,** 678–686 (1985). DOI: 10.1021/bi00324a021

10. Knighton, D. R.; Kan, C.-C.; Howland, E.; Janson, C. A.; Hostomska, Z.; Welsh, K. M.; Matthews, D. A. Electrostatic channeling in the bifunctional enzyme dihydrofolate reductase-thymidylate synthase. *Nat. Struct. Biol.* ***1***, 186–194 (1994). DOI: 10.1038/nsb0394-186

11. Elcock, A. H., Potter, M. J., Matthews, D. A., Knighton, D. R. & McCammon, J. A. Electrostatic channeling in the bifunctional enzyme dihydrofolate reductase-thymidylate synthase. *J. Mol. Biol.* **262,** 370–374 (1996). DOI: 10.1006/jmbi.1996.0520

12. Elcock, A. H., Huber, G. a. & Andrew McCammon, J. Electrostatic channeling of substrates between enzyme active sites: Comparison of simulation and experiment. *Biochemistry* **36,** 16049–16058 (1997). DOI: 10.1021/bi971709u

13. Lindbladh, C.; Rault, M.; Hagglund, C.; Small, W. C.; Mosbach, K.; Bülow, L.; Evans, C.; Srere, P. A. Preparation and kinetic characterization of a fusion protein of yeast mitochondrial citrate synthase and malate dehydrogenase. *Biochemistry* **1994**, *33* (39), 11692–11698. DOI: 10.1021/bi00205a004

14. Lindbladh, C., Brodeur, R. D., Small, W. C., Lilius, G., Bulow, L., Mosbach, K., Srere, P. A. Erratum: Metabolic studies on Saccharomyces cerevisiae containing fused citrate synthase/malate dehydrogenase. *Biochemistry* **33,** 11684-11691 (1994). DOI: 10.1021/bi00253a034

15. Moehlenbrock, M. J., Toby, T. K., Pelster, L. N. & Minteer, S. D. Metabolon catalysts: An efficient model for multi-enzyme cascades at electrode surfaces. *ChemCatChem* **3,** 561–570 (2011). DOI: 10.1002/cctc.201000384

16. Wheeldon, I.; Minteer, S. D.; Banta, S.; Barton, S. C.; Atanassov, P.; Sigman, M. Substrate channelling as an approach to cascade reactions *Nat. Chem.* **8**, 299–309 (2016). DOI: 10.1038/nchem.2459

17. Idan, O. & Hess, H. Engineering enzymatic cascades on nanoscale scaffolds. *Curr. Opin. Biotechnol.* **24,** 606–11 (2013). DOI: 10.1016/j.copbio.2013.01.003

18. Wilner, O. I.; Weizmann, Y.; Gill, R.; Lioubashevski, O.; Freeman, R.; Willner, I. Enzyme cascades activated on topologically programmed DNA scaffolds. *Nat. Nanotechnol.* **4**, 249–254 (2009). DOI: 10.1038/nnano.2009.50

19. Lin, J. L. & Wheeldon, I. Kinetic enhancements in DNA-enzyme nanostructures mimic the sabatier principle. *ACS Catal.* **3,** 560–564 (2013). DOI: 10.1021/cs300766d

20. Teller, C. & Willner, I. Organizing protein-DNA hybrids as nanostructures with programmed functionalities. *Trends Biotechnol.* **28,** 619–628 (2010). DOI: 10.1016/j.tibtech.2010.09.005

21. Niemeyer, C. M. Semisynthetic DNA-protein conjugates for biosensing and nanofabrication. *Angew. Chemie - Int. Ed.* **49,** 1200–1216 (2010). DOI: 10.1002/anie.200904930

22. Eun, C., Kekenes-Huskey, P. M., Metzger, V. T. & McCammon, J. A. A model study of sequential enzyme reactions and electrostatic channeling. *J. Chem. Phys.* **140,** (2014). DOI: 10.1063/1.4867286

23. Idan, O. & Hess, H. Origins of activity enhancement in enzyme cascades on scaffolds. *ACS Nano* **7,** 8658–8665 (2013). DOI: 10.1021/nn402823k

24. Fell, D. A. & Sauro, H. M. Metabolic control and its analysis. Additional relationships between elasticities and control coefficients. *Eur. J. Biochem.* **148,** 555–561 (1985). DOI: 10.1111/j.1432-1033.1985.tb08876.x

25. Kascer H., Burns, A. The Control of Flux. *Symp Soc Ex Biol* 65–104 (1973).

26. West, A. C. *Electrochemistry and Electrochemical Engineering*. (2013).

27. Fell, D. A. Metabolic control analysis: a survey of its theoretical and experimental development. *Biochem. J.* **286,** 313–30 (1992). DOI: 10.1042/bj2860313

28. Hamann, C. H., Hamnett, A. & Vielstich, W. *Electrochemistry*. (2007).

29. Metzger, V. T., Eun, C., Kekenes-Huskey, P. M., Huber, G. & McCammon, J. A. Electrostatic channeling in P. falciparum DHFR-TS: Brownian dynamics and Smoluchowski modeling. *Biophys. J.* **107,** 2394–402 (2014). DOI: 10.1016/j.bpj.2014.09.039

30. http://bit.ly/2bPbtgx

31. http://bit.ly/2bPc6GT

32. http://bit.ly/2cpeg5s

33. http://bit.ly/2bPbEZn